Dispersive Qubit Readout with Intrinsic Resonator Reset

Downloaded from: https://research.chalmers.se, 2026-11-15 15:48 UTC

Citation for the original published paper (version of record):
Jerger, M., Motzoi, F., Gao, Y. et al (2026). Dispersive Qubit Readout with Intrinsic Resonator Reset. PRX Quantum, 7(3). http://dx.doi.org/10.1103/z5x1-2mr9

N.B. When citing this work, cite the original published paper.

research.chalmers.se offers the possibility of retrieving research publications produced at Chalmers University of Technology. It covers all kind of research output: articles, dissertations, conference papers, reports etc. since 2004. research.chalmers.se is administrated and maintained by Chalmers Library

(article starts on next page)

Dispersive Qubit Readout with Intrinsic Resonator Reset

M. Jerger,[1,*] F. Motzoi,[2,3,†] Y. Gao,[4] C. Dickel,[5] L. Buchmann,[6] F. A. Cárdenas-López,[2] A. Bengtsson,[7] G. Tancredi,[7] C. W. Warren,[7] J. Bylander,[7] D. DiVincenzo,[8] R. Barends,[4] and P. A. Bushev[1,‡]

[1]*Institute for Functional Quantum Systems (PGI-13), Forschungszentrum Jülich, 52425 Jülich, Germany*
[2]*Institute of Quantum Control (PGI-8), Forschungszentrum Jülich, 52425 Jülich, Germany*
[3]*Institute for Theoretical Physics, Universität zu Köln, Zülpicher Str. 77, 50937 Köln, Germany*
[4]*Department of Physics, RWTH Aachen University, 52074 Aachen, Germany*
[5]*Physikalisches Institut II, Universität zu Köln, Zülpicher Str. 77, 50937 Köln, Germany*
[6]*Department of Physics and Astronomy, Aarhus University, 8000 Aarhus, Denmark*
[7]*Microtechnology and Nanoscience, Chalmers University of Technology, SE-412 96 Göteborg, Sweden*
[8]*JARA-Institute for Quantum Information (PGI-11), Forschungszentrum Jülich, 52425 Jülich, Germany*

(Received 24 July 2024; revised 19 December 2025; accepted 8 July 2026; published 31 August 2026)

Measurement and readout speed impose limits for logical qubit and qudit performance in quantum computing. Here, we experimentally demonstrate a universal analytical method for designing bandwidth-efficient dispersive readout pulses that intrinsically reset the resonator and extend it to multiple quantum states. The approach is based on universal analytical pulses and requires knowledge of the qubit and resonator parameters, but needs no direct optimization of the pulse shape, even when accounting for the nonlinearity of the system. When correcting for the Kerr nonlinearity, we find even more precise solutions to the speed-versus-photon-number trade-off, achieving 10^2 photon readout with reset to 10^{-2} within $3\kappa^{-1}$ duration and amplifier efficiency- and T_1-limited assignment error around 0.6%. Results on qubits and qutrits validate the approach.

DOI: 10.1103/z5x1-2mr9

I. INTRODUCTION

One of the key challenges for scalable quantum computing is speeding up the repetitive measurement and initialization process required for quantum error correction (QEC) algorithms [1–3]. Fast measurements will decrease readout error as well as reduce decoherence associated with cycle times in QEC. In superconducting quantum systems, however, the measurement speed is typically orders of magnitude slower than one- and two-qubit gates, which have otherwise reached the 10 ns timescale [4–8]. A critical complication is that after a measurement, a state-dependent residual intra-cavity field holds up the QEC cycle for a time dramatically exceeding the cavity decay time $\tau_c = \kappa^{-1}$. This residual intra-cavity field shifts the resonance frequency of the qubit via ac-Stark interaction, which interferes with subsequent operations and causes decoherence [9]. To mitigate these effects, the gate set or circuit compiler has to add extra waiting times to empty the cavity between operations [8,10–12].

A valuable resource for QEC algorithms is having a short cavity ring-down time τ_c for dispersive readout, so that algorithms can resume immediately. There are a couple of methods for the fast depletion of the intra-cavity field. For example, a fast cavity ($\kappa^{-1} \approx 10$ ns) coupled to a Purcell filter allows for a high fidelity readout with 0.25% assignment error within 88 ns [5]. Recently, non-linear Purcell filters have been explored to fix the trade-off between residual intra-cavity photon noise and fidelity [13]. An optimized cavity-qubit design is used for the multiplexed qubit readout in QEC [10]. The optimization of tailored multi-step pulse shapes [14] or a feed-forward technique with state-dependent depletion pulses may furthermore be used for the fast depletion of the intra-cavity field [15]. However, an approach that natively integrates rapid measurement with the cavity reset and straightforwardly allows for scaling up the complexity of quantum circuits, including linear as well as non-linear elements, remains an open challenge.

In this article, we present a simple readout method that combines fast single-shot measurement with state-independent nulling of the readout cavity field using analytical pulses. When taking into account the qubit-induced Kerr non-linearity we demonstrate more than a

*Contact author: m.jerger@fz-juelich.de
†Contact author: f.motzoi@fz-juelich.de
‡Contact author: p.bushev@fz-juelich.de

Published by the American Physical Society under the terms of the Creative Commons Attribution 4.0 International license. Further distribution of this work must maintain attribution to the author(s) and the published article's title, journal citation, and DOI.

10^3-fold residual cavity field reduction immediately after the pulse and an assignment error of 0.6% within a total readout duration of $3\kappa^{-1}$. We also show a three-state readout since the method generalizes to arbitrary numbers of modes and states.

II. EXPERIMENTAL DEMONSTRATION OF READOUT WITH CAVITY RESET

A. Transmon device

We experiment with a conventional circuit QED setup consisting of a fixed frequency transmon qubit coupled to a half-wavelength resonator, see the simplified sketch in Fig. 1(a). The resonance frequency of the qubit is measured to be $\omega_{01}/2\pi = 3947$ MHz with anharmonicity $\alpha/2\pi = -232$ MHz, $T_1 \approx 40$–75 μs and $T_2^* \approx 20$–40 μs, varying over time. The resonance frequency of the readout cavity is $\omega_c/2\pi = 6041.200$ MHz and its linewidth is $\kappa/2\pi = 0.5647(3)$ MHz, corresponding to the time constant of $\tau_c = \kappa^{-1} = 281.2(8)$ ns. The dispersive shift of the resonator is $\chi/2\pi = 0.299(1)$ MHz. These numbers are subject to small variations between experimental runs due to the aging of the device. A detailed description of the chip can be found in Ref. [16] and a description of the experimental setup is presented in Appendix A. The device was fabricated at Myfab Chalmers.

B. Readout with cavity reset. Concept

In the dispersive regime, the Hamiltonian of the qubit-cavity system under excitation of the input field in the rotating frame is well approximated by $\hat{H}_d = \hbar(\Delta + \chi\hat{\sigma}_z)\hat{a}^+\hat{a}$, where $\Delta = \omega_c - \omega_{01}$ is the qubit-cavity detuning. Since the cavity is excited with coherent pulses through the input port, the quantum noise of the microwave signal is additive white vacuum noise, which averages to zero, and we can neglect noise operators in our notation. In this simplification, all functions can be considered the expectation value of coherent optical states, and the resonator is described by the classical state-dependent response functions [17]. Thus, the relation between input $a_{\text{in}}(t)$ and cavity fields $a(t)$ in the time domain is described in terms of linear response theory [18] by Duhamel's integral [19]

$$a(t) = \frac{1}{\sqrt{\kappa}}\int_{-\infty}^{\infty} h(t-\tau)a_{\text{in}}(\tau)d\tau, \tag{1}$$

where $h(t)$ is the time-domain response function of the resonator. Here, the function $h(t)$ is normalized to $\int_{-\infty}^{\infty}|h(t)|^2dt = \kappa/2\pi$.

The Fourier transformation of Eq. (1) yields the resonator response in frequency space and reads as

$$a(\omega) = h(\omega)a_{\text{in}}(\omega)/\sqrt{\kappa}, \tag{2}$$

$$h(\omega) = \kappa/(\kappa/2 + i(\omega - \omega_i)), \tag{3}$$

where ω_i is the state-dependent resonance frequency of the cavity with the boundary condition $a_{\text{out}}(\omega) = \sqrt{\kappa}a(\omega) + a_{\text{in}}(\omega)$ [20,21].

Figure 1(b) demonstrates the response of the cavity to a conventional rectangular (no smoothed edges) readout pulse of $T_p = 1$ μs duration. The process of the slow initial building of the intra-cavity field $\langle n(t)\rangle = |a(t)|^2$ is followed by its long decay with the time constant of κ^{-1}. It takes $10\kappa^{-1}$ until it fades in the detection noise level corresponding to $\simeq 5\times 10^{-3}$ intra-cavity photons. The dark solid line represents the fit of the experimental data to the response theory described above, where the setup's input and output transmission amplitudes and phases were the only fitting parameters with the known resonator's ω_c and κ.

Following up on the shortly outlined theory represented by Eqs. (1)–(3), it is possible to tailor an input signal $a_{\text{in}}(t)$ that resets the cavity to its initial state at its end [22]. For that, we choose the desired cavity response $a = a_T(t)$, referred to as the trial function, that satisfies $a_T(t) = 0 \quad \forall\ t \le 0, t \ge T_p$. The input field that generates this cavity response when the qubit is in its ground state can then be calculated by using the inverse Fourier transform:

$$a_{\text{in}}(\omega) = \sqrt{\kappa}h^{-1}(\omega)a_T(\omega), \tag{4}$$

$$a_{\text{in}}(t) = \left[\kappa/2 - i\chi_0 + \frac{d}{dt}\right]a_T(t)/\sqrt{\kappa}. \tag{5}$$

The condition that $a_{\text{in}}(t)$ be finite-valued and have finite duration T_p implies first-order smoothness of $a_T(t)$ and

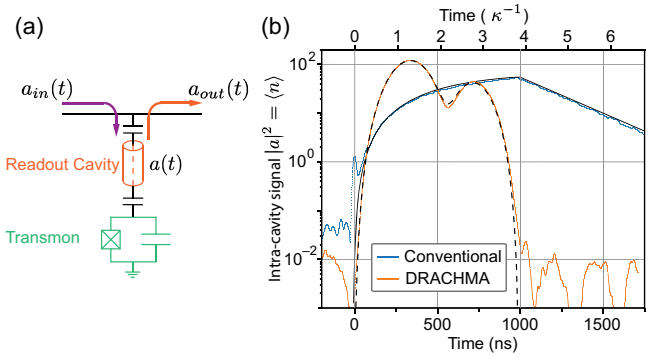

FIG. 1. (a) Simplified circuit diagram for the demonstration of dispersive readout of a superconducting qubit. (b) Demonstration of the concept of readout with cavity reset. Blue: the rectangular input readout pulse of duration $T_p = 1$ μs causes a long exponential decay of the intra-cavity field $|a(t)|^2$. The solid line represents a fit of experimental data to a classic response theory, see Eq. (1). Orange: the DRACHMA readout with the Kerr-corrected pulse of the same length $T_p = 1$ μs quickly drives the cavity and returns it to the initial state. The dashed line represents a fit of experimental data to theory, see Eqs. (9) and (10).

$\dot{a}_T(0) = \dot{a}_T(T_p) = 0$. Here, we consider all equations in the rotating frame at carrier frequency, thus $\chi_0 = \omega_0 - \omega_{\text{carrier}}$. We refer to this technique as Derivative Removal for Annulment of Cavity-Hybridized Measurement Adiabats (DRACHMA). To demonstrate the concept we plot on Fig. 1(b) the example of the cavity response to such a DRACHMA pulse of $T_p = 1$ μs duration. The readout pulse quickly drives the cavity to the maximum number of photons $\langle n \rangle \sim 10^2$ and returns it to $\langle n \rangle \sim 10^{-2}$ when the pulse is over.

C. Readout with cavity reset. No Kerr correction

An example of DRACHMA readout of a single quantum state (ground) is shown in Fig. 2(a). The input signal $a_{\text{in}}(t)$ of $T_p = 1$ μs duration is analytically derived by using Eq. (5) from the trial response function $a_T(t) = \sin^3 \pi t/T_p$ which satisfies the smoothness condition at the pulse boundaries. Both quadratures of the generated smooth input signal are displayed in the same figure. The input signal is applied at the carrier frequency halfway between the resonator frequencies corresponding to the ground and excited states of the transmon.

When the transmon is prepared in $|0\rangle$, see Fig. 2(a), the DRACHMA readout causes a 20 dB partial reset of the intra-cavity field to $|a(t)|^2 \simeq 10^{-1}$ photons. Immediately after the pulse, the intra-cavity field experiences the conventional exponential decay. However, when the qubit is prepared in $|1\rangle$, the readout with DRACHMA pulse works as the ordinary pulse (as plotted in Fig. 1). It reaches 10^{-1} photons within $6\kappa^{-1}$ after the end of the pulse.

The above-presented readout technique can be generalized to an arbitrary number of quantum states N in the following way:

$$a_{\text{in}}(\omega) = \sqrt{\kappa}\left[\prod_{j=0}^{N-1} h_j^{-1}(\omega)\right] a_T(\omega), \tag{6}$$

$$a_{\text{in}}(t) = \sqrt{\kappa}\left[\prod_{j=0}^{N-1}\left(\kappa/2 - i\chi_j + \frac{d}{dt}\right)\right] a_T(t)/\kappa^N, \tag{7}$$

with $h_j(\omega) = \kappa/(\kappa/2 + i\omega - i\chi_j)$ being the frequency-domain transfer functions for the particular quantum state $|j\rangle$ with dispersive shift χ_j with respect to the carrier frequency. To satisfy the smoothness condition, the trial function $a_T(t)$ and its first N derivatives must all vanish at $t = 0$ and $t = T_p$. An example of such a smooth response function is $a_T(t) = \sin^m(\pi t/T_p)$, where the exponent $m > N$.

Figure 2(b) shows the DRACHMA readout of the qubit. The readout pulse $a_{\text{in}}(t)$ is analytically calculated from the trial function $a_T(t) = \sin^3(\pi t/T_p)$ with experimentally determined state-dependent dispersive shifts $\chi_{0,1} = \pm\chi$ and cavity decay κ^{-1}. The length of the pulse is set to $T_p = 1$ μs. The trajectory of the intra-cavity field for both states follows the optimized pulse shape during the readout

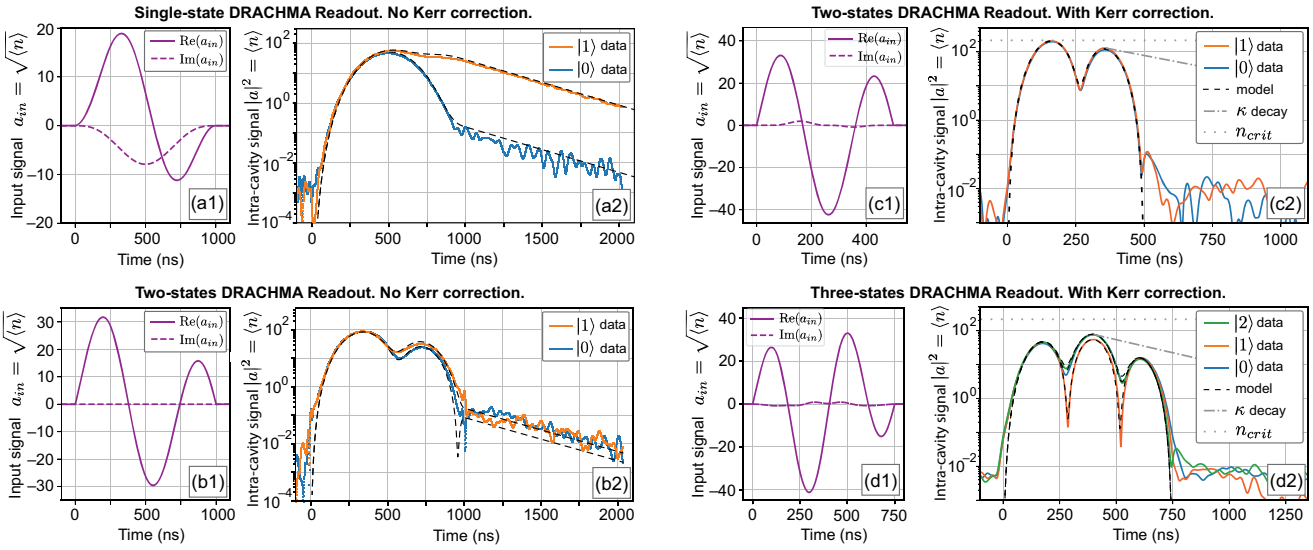

FIG. 2. DRACHMA input fields $a_{\text{in}}(t)$ and the dynamics of intra-cavity fields $\langle n(t) \rangle \propto |a(t)|^2$. (a) Readout with cavity reset for a single state. (b) Readout with cavity reset for the ground and first excited states of the transmon. (c),(d) DRACHMA readout when Kerr-nonlinearity corrections are taken into account. (c) Readout with > 35 dB cavity reset for the ground and first excited states of the transmon with $T_p = 500$ ns. (d) Readout with > 30 dB cavity reset for the ground, excited and second excited (qutrit) states with $T_p = 750$ ns. Solid lines are experimental data, and black dashed lines represent fits to the theory. The dash-dotted line (κ decay) shows the conventional exponential decay of the readout cavity from the top of the pulse with decay constant κ^{-1}. The gray dotted line indicates the field magnitude corresponding to the critical photon number n_{crit}.

pulse duration, resulting at the end of the pulse in the 20 dB cavity reset to 10^{-1} microwave photons. After the end of the readout pulse, the residual intra-cavity field demonstrates conventional exponential decay. The evolution of the intra-cavity fields for the ground and excited states $a_{0,1}(t)$ is very well fit by the theory where the amplitudes and phases of transmission of the input and output of the setup were the only fitting parameters.

D. Readout with cavity reset. With Kerr correction

The performance of the above-described readout technique is limited by the additional non-linear shift of the resonator frequency at a relatively strong coherent drive [23]. To achieve the highest measurement contrast with shorter readout pulses, we need to drive the cavity closer to the critical number of photons $n_{\mathrm{crit}} \simeq 200$. In that case, the system's Hamiltonian needs to include the Kerr non-linear term: $\hat{H}_{\mathrm{tot}} = \hat{H}_d + \hbar\zeta\hat{\sigma}_z(\hat{a}^+)^2\hat{a}^2$, where ζ is a state-dependent Kerr constant [24]. In the semi-classical limit, i.e. in the case of the strong coherent intra-cavity field $a(t) = \langle\hat{a}(t)\rangle \gg 1$, we employ the polaron displacement $\hat{a} \to \hat{a} + a(t)$. This results in the effective time-dependent "mean-field" Hamiltonian

$$\hat{H}_{\mathrm{eff}} = \hbar\Delta\hat{a}^+\hat{a} + \hbar(\chi + 4\zeta|a(t)|^2)\hat{\sigma}_z\hat{a}^+\hat{a}, \tag{8}$$

which contains an additional term describing the power-dependent frequency shift of the resonator.

We use an iterative approach for the incorporation of the non-linear shift into the above-described optimized DRACHMA readout. At first, we calculate the actual intra-cavity field of the Kerr-unperturbed resonator at the ground and excited states by using Eq. (7) for the trial function $a_T(t) = \sin^3(\pi t/T_p)$.

$$\tilde{a}_{0,1}(t) = \left[\kappa/2 - i\chi_{1,0} + \frac{d}{dt}\right]a_T(t)/\kappa. \tag{9}$$

For the second iteration, the Kerr-perturbed resonator frequencies at the ground and excited states are used for the calculation of the actual input pulse by using the same Eq. (7):

$$a_{\mathrm{in}}(t) = \left[\prod_{j=0}^{1}\left(\frac{\kappa}{2} - i(\chi_j + 4\zeta_j|\tilde{a}_j(t)|^2) + \frac{d}{dt}\right)\right]a_T(t)/\kappa^{3/2}. \tag{10}$$

The readout of the transmon qubit with the Kerr-corrected DRACHMA pulse of $T = 500$ ns $(\simeq 2\kappa_c^{-1})$ duration is shown in Fig. 2(c). The pulse is rather strong and causes the intra-cavity field to reach the critical photon number n_{crit}. The non-linear constants are determined during an optimization routine. At first, both Kerr constants $\zeta_{0,1}$ are set to zero. Then, we perform an incremental scan for both ζ at a fixed magnitude and duration of the readout pulse while finding the optimal parameter range that results in the maximum depletion of the residual intra-cavity field directly after the pulse. In the presented experiment, the optimal Kerr constants $\zeta_0/2\pi = -175$ Hz and $\zeta_1/2\pi = -56$ Hz are comparable to the first-order theoretical estimated value $\tilde{\zeta} = -g^4/\Delta^3 \approx -50$ Hz. The experimental application of non-linear terms via the DRACHMA method results in the immediate, i.e. faster than κ^{-1}, cavity reset right after the end of the readout pulse even at high photon numbers. The intra-cavity field $a(t)$ demonstrates a significant 35 dB drop to the noise level of the detection system corresponding to $n \simeq 5 \times 10^{-3}$ in the cavity.

E. Readout of three states with cavity reset

The level structure of our transmon device allows for the demonstration of DRACHMA readout for the case of three states, see Fig. 2(d). For that purpose, we initially determine the dispersive shifts $\chi_0/2\pi = 0.598$ MHz, $\chi_1 = 0$ and $\chi_2/2\pi = -0.497$ MHz relative to the cavity frequency in the first excited state of the qubit and the remaining Kerr constant $\zeta_2 = 60$ Hz. We use the trial function $a_T(t) = \sin^4(\pi t/T_p)$ with a pulse duration of 750 ns together with non-linear terms to achieve practically an instant reset of the intra-cavity field, where the intra-cavity field drops by more than 30 dB magnitude with respect to the conventional exponential decay (dash-dotted line κ-decay) with time constant τ_c.

F. Readout signal optimization

Figure 3 shows the evolution of the intra-cavity field in the IQ plane during the readout pulse. The horizontal and vertical axes represent the in-phase and quadrature components of the cavity field measured in units of the square root of intra-cavity photon number. The measured trajectories correspond to the cavity response for the qubit in the nominal ground ($|0\rangle$-blue), 1st excited ($|1\rangle$, orange) and 2nd excited ($|1\rangle$, green) states, while the dashed black lines indicate the theoretical model.

During the readout pulse, the cavity field follows distinct trajectories for the two qubit states, reflecting the state-dependent dispersive shift of the cavity. Due to the pulse engineering, the state information is confined primarily to the Q quadrature, which would enable readout improvements with a phase-sensitive parametric amplifier. Notably, both trajectories start and end at the origin, indicating that the pulse shape leaves no residual photons in the resonator after the measurement. This property minimizes dephasing and means the readout pulse can be immediately followed by operations, such as a reset or the gates required in quantum error correction cycles.

Figure 4(a) demonstrates the time evolution of the measured in-phase quadrature of the qubit readout signal

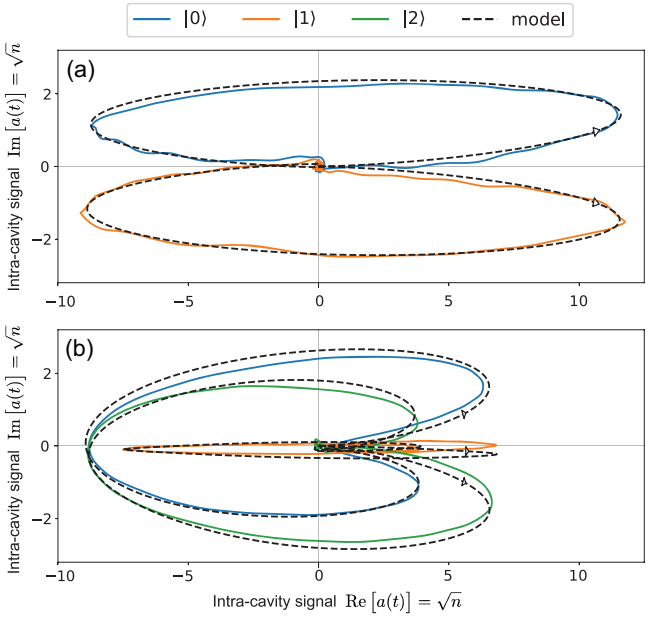

FIG. 3. Time evolution of the intracavity field in the IQ plane during qubit readout for (a) two-states readout and (b) three-states readout. The horizontal $\mathrm{Re}[a(t)]$ and vertical $\mathrm{Im}[a(t)]$ axes correspond to the in-phase and quadrature components of the intra-cavity field, both proportional to the square root of the intra-cavity photon number. The trajectories shown for the qubit in the ground ($|0\rangle$, blue), 1st excited ($|1\rangle$, orange) and 2nd excited ($|1\rangle$, green) states follow distinct paths, while the dashed black lines represent the theoretical model. Both trajectories start and end at the origin, indicating that the optimized pulse shape leaves no residual photons in the resonator after measurement.

when applying Kerr-corrected DRACHMA pulses of various durations from 250 to 1500 ns. The magnitude of the input pulses is chosen to yield the same number of intra-cavity photons for all pulse durations. The acquired quadrature signals are digitally low-pass filtered with the cutoff frequency of 40 MHz and averaged over 10^6 repetitions of the experiment. In the case of qubit measurements, the DRACHMA readout signal is engineered in such a way that it is proportional to the trial function

$$Z_{\mathrm{RO}}(t) \propto i(a_1(t) - a_0(t)) = 2a_T(t)\chi/\kappa. \tag{11}$$

Equation (11) and Fig. 4(b) demonstrate clearly that, for a purely real or purely imaginary a_T, the readout signal is mainly contained in one of the quadratures. The technique is therefore compatible with homodyne measurement, which can potentially double the measurement efficiency at the cost of using a single frequency. At very short T_p the growing derivative terms of a_{in} increase the maximum photon number in the cavity but not the rate of information extracted from the qubit so that the readout signal diminishes faster than linear in T_p if the maximum number of photons in the cavity is held constant, as seen in Fig. 4(c). This can be mitigated by increasing χ and κ.

G. Single-shot performance

To further quantify the performance of the DRACHMA readout, we now measure the assignment fidelity $\mathcal{F}_a$. We carry out a series of single-shot measurements of the qubit with Kerr-corrected pulses of different durations. In these experiments, the acquired readout signals $a_{\mathrm{out}}(t)$ are multiplied with the analytically calculated complex-valued weighting function $W(t) = [Z_{\mathrm{RO}}(t)]^*$ for the specific pulse shape and integrated. We perform 10^6 repetitions of the experiment while preparing a desired quantum state for each pulse length. The resulting ground and excited state histograms are simultaneously fitted to the sum of two Gaussians. From this fit, we determine a measurement assignment error $1-\mathcal{F}_a = \frac{1}{2}[P(1|0)+P(0|1)]$, see Ref. [25] and plot it as a function of readout pulse duration, see Fig. 5(a). The green circles correspond to the readout, which minimizes the assignment error, and red squares

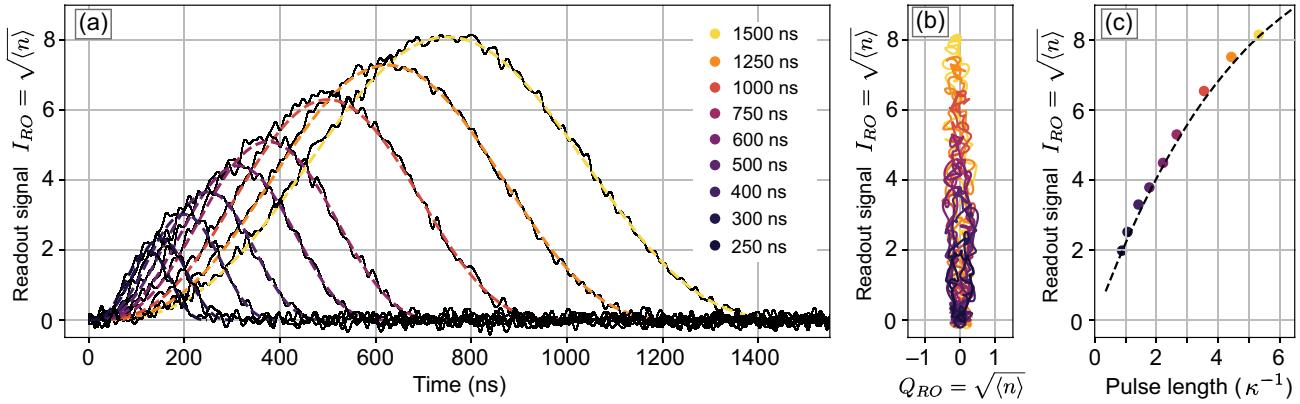

FIG. 4. (a) The measured in-phase readout signal $I_{\mathrm{RO}} = \mathrm{Re}[Z_{\mathrm{RO}}(t)]$ for the various durations of the DRACHMA pulse between 250 and 1500 ns. The magnitude of the input signal results in the same number of photons at the maximum of the intra-cavity field. (b) The evolution of the measured readout signal in the IQ plane. (c) The maximum of the readout signal as the function of the pulse duration. The dashed lines show the theoretical predictions from input-output theory.

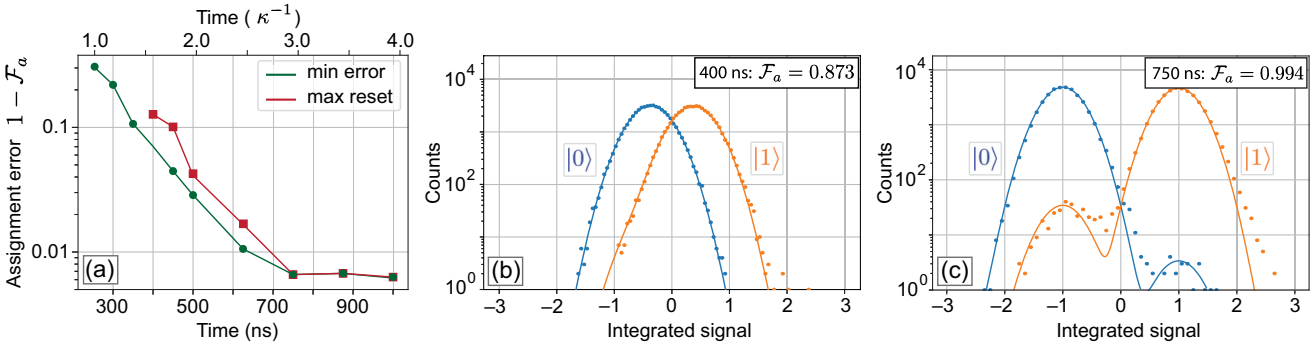

FIG. 5. (a) Best achieved state assignment error $1-\mathcal{F}_a$ as a function of the DRACHMA pulse length for two cases: any pulse amplitude (green circles), amplitudes where >35 dB reset contrast is maintained (red squares). (b),(c) Experimentally measured histograms of the integrated readout quadrature signal for measurement pulse lengths of $T_p = 400$ ns and $T_p = 750$ ns and >35 dB reset contrast. The use of a longer pulse results in better state distinguishability.

indicate the case when the cavity experiences a reset by more than 35 dB. For $T_p < 400$ ns the available driving amplitude is insufficient to reach photon numbers of more than 35 dB above the noise level. In both cases, the decrease in the assignment error reflects the increase in the information signal for a longer period of the readout/integration time [5]. The assignment error reaches its minimal level of 0.6% for readout durations between 2.7 and 3.5 κ^{-1}.

Figures 5(b) and 5(c) demonstrate the experimentally measured histograms of the integrated readout quadrature for the pulse duration of 400 and 750 ns. The magnitude of the readout signal is chosen such that the intra-cavity field attains the critical number of photons. The specific signal shape also results in the significant >30 dB suppression of the intra-cavity field. The assignment error experiences some fluctuations in the level of $\simeq 0.2\%$ which can be attributed to the fluctuations of T_1. We believe that the experimentally demonstrated high assignment fidelity is still largely limited by the low χ and low amplifier efficiency (17%), and increasing these would likely boost the assignment fidelity further.

H. DRACHMA readout with Purcell filters

The method can also more generally be applied to quantum networks [28] involving linear or weakly nonlinear elements. Purcell filters are used to tailor the noise of measurement cavities, thus better isolating and extending the lifetimes of superconducting qubits. In-depth studies can be found in Refs. [26,29], but the essence is that by introducing a second cavity at the output of the first, different rates of decay can be obtained for the qubit frequency as opposed to its resonator. This can greatly reduce qubit decay while not trapping light for too long. The network arrangement consists of two coupled cavities in series, with input and output ports of the measurement field occurring on single cavities. The two intracavity fields obey [26]

$$\begin{aligned}\dot{C}_1(t) &= i(\Delta+\chi_j)C_1(t) + iGC_2(t) + i\sqrt{\kappa}a_{\text{in}}(t),\\ \dot{C}_2(t) &= i\delta C_2(t) + iG^*C_1(t) - \frac{\kappa}{2}C_2(t),\end{aligned} \tag{12}$$

with C_i the intra-cavity fields of the cascaded system, δ the detuning between the cavities, G the capacitive coupling between the cavities, Δ the detuning to the driving field, κ the bare decay rate of the Purcell cavity, and a as before the amplitude of the driving (measurement) field.

In frequency space, this correspond to

$$\begin{aligned}C_1(\omega) &= (i\sqrt{\kappa}a_{\text{in}}(\omega) + iGC_2(\omega))/(i\omega - i\Delta - i\chi_j)\\ C_2(\omega) &= iG^*C_1(\omega)/(\kappa/2 + i\omega - i\delta).\end{aligned} \tag{13}$$

Note that if the cavities were uncoupled this would correspond to three modes, two for the first cavity (split by the qubit state) and a third for the Purcell cavity. Because the cavities are coupled this results in further splitting, leaving us with four hybridized network modes. Solving the equation system for the network output field gives

$$\begin{aligned}a_{\text{out}}^{|j\rangle}(\omega) &= \sqrt{\kappa}C_2(\omega)\\ &= \frac{-\kappa G^*}{(i\omega - i\Delta - i\chi_j)(\kappa/2 + i\omega - i\delta) + |G|^2}a_{\text{in}}(\omega).\end{aligned} \tag{14}$$

This arrangement has the advantage that larger environmental couplings (κ, G) can be achieved for the light; however, there remains a mild trade-off with qubit lifetime. Moreover, while the coupling can be stronger, it has been a challenge to define piecewise-constant sequences for reset protocols in these more complex dynamics.

To ensure adiabatic passage regardless of the measured state, we can, however, straightforwardly modify the

smooth input a_{in} to

$$a_{\text{in}}(\omega) = \sqrt{\kappa} a_T(\omega) h_{|0\rangle}^{-1} h_{|1\rangle}^{-1}$$
$$G\kappa h_{|j\rangle}^{-1} = (i\omega - i\Delta - i\chi_j)(\kappa/2 + i\omega - i\delta) + |G|^2, \quad (15)$$

which ensures once again that the output is purely polynomial in ω and thus adiabatic and non-destructive to the cavity. The performance of the pulse is compared to that of standard Gaussian pulse measurement and plotted in Fig. 6 using the parameters from Refs. [26,27]. We see that within the power limits of the system, loosely defined as staying within the boundaries of n_{crit}, DRACHMA is able to suppress the leftover population in the network. In multiplexed devices, it is often the Purcell cavity C_2 that is driven rather than C_1. This should not affect the overall dynamics [26].

The combination of DRACHMA and Purcell filters would thereby enable the simultaneous suppression of intra-cavity population, while also suppressing qubit (Purcell) relaxation. Similar techniques could be used for other network arrangements, such as in generating remote entanglement by postselection [30–32] or potentially measurement-based feedback [33], where transient tails can dramatically reduce concurrence [34].

I. Accelerated dispersive readout and relative speedup

Table I summarizes a selection of representative dispersive readout experiments from the literature, together with the present work. To enable a fair comparison across distinct experimental platforms, we express all relevant timescales in units of the cavity decay constant, κ. This dimensionless representation highlights the relative speed of the readout process, independent of the specific cavity linewidth, coupling strength, or photon number used in each setup. Because the term "fast" is ambiguous in absolute units, our analysis focuses instead on the *relative acceleration* of the readout process with respect to the natural cavity timescale. Note that we have also independently numerically checked that keeping κ fixed and varying the readout time while maintaining comparable SNR likewise gives a significant speedup for comparable error. An example of such a same-SNR comparison is given in Appendix F.

Our pulse design achieves a complete readout and cavity reset within $(T_p + T_{\text{hold}})\kappa \approx 3$, corresponding to a roughly sevenfold acceleration compared to conventional Gaussian or rectangular envelope readouts that typically require $(T_p + T_{\text{hold}})\kappa \gtrsim 20$ for comparable fidelity.

Within the dispersive approximation, there is no privileged timescale. The measurement rate scales as $n_{\text{crit}}\kappa$, and for the optimal readout χ and κ are proportionally related [5,42]. It is possible to increase n_{crit} by making χ smaller, and hence at the cost of proportionally decreasing of κ, but then the measurement time is correspondingly increased. Driving the readout cavity far beyond n_{crit} is not optimal, because there is apparently a universal behavior that at higher photon number the system completely loses controllability [43].

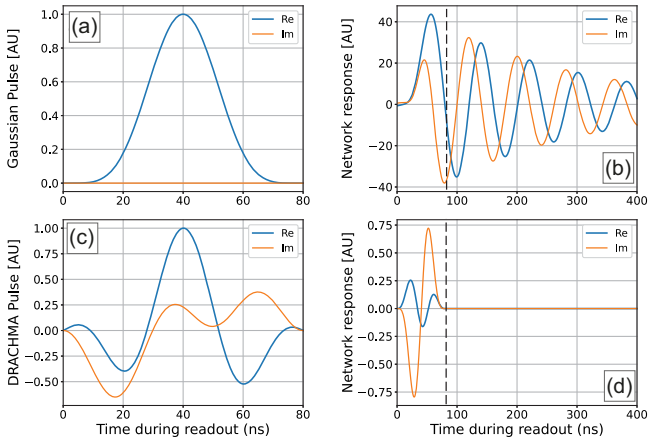

FIG. 6. Relationship between the Purcell network mode population and the input readout pulse. In (a) and (b) a standard Gaussian measurement pulse is simulated, while in (c) and (d) the DRACHMA pulse (15) is used. In the left column the pulses are plotted for an 80 ns readout, while in the right column the time-domain response is, respectively, shown. The dashed line indicates the end of the readout pulse. Without correction, the network mode requires a much longer time to empty than expected from the bare cavity linewidth. Non-linearity is not included in the simulation but would not be visible on the linear grid plot. Parameters are $G/2\pi = 20$ MHz, $\kappa/2\pi = 14$ MHz, $\delta/2\pi = 50$ MHz, $\chi/2\pi = 6$ MHz, taken from Refs. [26,27].

TABLE I. Comparison of dispersive measurement performance across several readout experiments. The additional **QND** column indicates whether the state can be reused afterward, as in mid-circuit measurement. The asterisks indicate that no hold time (T_{hold}) was reported to allow the cavity population to decay (10^4-fold), but adding it would in certain cases enable QND readout. Entries are sorted by decreasing measurement error.

Work	$1/\kappa$ (ns)	T_p (ns)	T_{hold} (ns)	Error	$(T_p + T_{\text{hold}})\kappa$	QND?
[8]	160	1500	3500	5.0%	31.2	Yes
[23]	20	80	250	3.0%	16.5	Yes
[35]	15	30	300	2.7%	22.0	Yes
[36]	100	750	1000*	2.2%	17.5	Yes*
[37]	45	n/a	300	2.0%	>6.7	Yes
[38]	17	300	170*	1.3%	27.6	Yes*
[15]	250	400	2500*	1.2%	11.6	Yes*
[12]	17	300	170*	1.1%	27.6	Yes*
[27]	37	140	370*	1.0%	13.8	Yes*
[5]	5	88	50*	0.80%	27.6	No*
Here	250	750	0	0.60%	3.0	Yes
[39]	10	100	100*	0.25%	20.0	Yes*
[40]	5	56	96	0.20%	32.5	Yes
[41]	85	320	170*	0.07%	5.8	Yes

There is an apparent trade-off: Measuring too slowly induces T_1 relaxation error of the qubit, and hence it will reduce the signal-to-noise ratio. On the other hand, measuring too fast would introduce additional errors such as state mixing, qubit driving, and other qubit-resonator interaction effects. There is strong evidence that this can be partially mitigated by increasing both cavity-qubit detuning and coupling as much as possible and hence becoming more dispersive. Regardless, it does not directly solve the problem of optimal drive power, since both qubit relaxation and non-dispersive interaction effects will remain and form a trade-off, and the optimum will depend on how much the coherent interaction effects can be suppressed, e.g. via pulse shaping. And if the solution is to make the system more dispersive, as in the current consensus, then this is precisely where DRACHMA pulses work the best and speed up the most.

As a quick example of this trade-off, the work [39] does indeed achieve sub-100 ns integration times with 0.25% infidelity, but including the idling time for the cavity (network) reset of roughly another 100 ns, this gives total dimensionless times of about $20/\kappa$ (i.e., about 7 times slower than our pulses would do for their system units), with similar conclusions for the works [12] and [5]. Additionally, by taking into account the better TWPA amplifier used in these experiments, resulting in 60%–70% efficiency versus 17% in ours, it is far from clear that the shorter times would generally work better. If the signal-to-noise ratio could directly be improved by threefold just by swapping out amplifiers, our measurement error would drop proportionally, by more than half, and well below 0.25%. That is, based purely on our own experimental long-duration parameters, we see our readout pulse shapes already work extremely well compared with the experiments mentioned above having integration times near 100 ns (without even accounting for 100–300 ns more for comparable photon suppression). If going to higher drive power, larger κ, and faster absolute speed, as in Refs. [5,12,39], does indeed help, then this would benefit lowering errors even further.

While the ultimate limit of readout fidelity will depend on system-dependent parameters such as amplifier efficiency and intrinsic T_1 relaxation, the present results show that, for a given κ, χ, and photon number, substantial speedup in $(T_p + T_{\mathrm{hold}})\kappa$ can be achieved solely through optimized pulse shaping. This relative improvement can directly translate into faster feedback loops and higher repetition rates in QEC algorithms in multi-qubit architectures, making the approach especially relevant for next-generation error-corrected and noisy intermediate-scale quantum systems.

III. CONCLUSION

The presented DRACHMA readout method can be easily applied to any other physical realization of a quantum system dispersively coupled to a readout resonator system such as ions [44], atoms [45,46], optomechanics [47], spins in solids [48], and semiconductor devices [49].

In conclusion, we have demonstrated a fast and high-fidelity dispersive readout of a transmon qubit with intrinsic cavity reset. Importantly, our approach for cavity reset uses analytical pulses. Moreover, only two essential parameters are needed: the dispersive shifts χ_j of the cavity and its decay rate κ. And finally, our method requires no complex optimization [14]. The crucial step in our method is the introduction of the qubit-induced non-linearity, which allows deployment of short pulses of large amplitudes. The presented methodology provides strong and rapid suppression of the cavity ring-downs, and it is well suited for direct implementation at scale in QEC [8,10,12].

ACKNOWLEDGMENTS

This work is supported by the EU through the HORIZON-CL4-2022-QUANTUM-01-SGA Project under Grant No. 101113946 OpenSuperQPlus100 and HORIZON-CL4-2021-DIGITALEMERGING-02-10 Grant Agreement 101080085 QCFD, by DPG under Germany's Excellence Strategy—Cluster of Excellence Matter and Light for Quantum Computing (ML4Q2) EXC 2004/2–390534769, by the BMBF through the project 13N15685 (GEQCOS), and within the framework program "Quantum technologies—from basic research to market" (Project QSolid, Grant No. 13N16149). We also acknowledge funding from the Knut and Alice Wallenberg Foundation.

DATA AVAILABILITY

The data that support the findings of this article are not publicly available. The data are available from the authors upon reasonable request.

APPENDIX A: EXPERIMENTAL SETUP

The experimental setup and a photograph of the superconducting chip are shown in Fig. 7. The superconducting device is packaged, protected from spurious magnetic noise by aluminum and cryoperm μ-metal shields and thermally anchored to the mixing chamber of the BlueFors XLD dilution refrigerator. The qubit control drive is synthesized by a Zürich Instruments HDAWG signal generator in the baseband, upconverted to the qubit frequency, attenuated, and applied to the charge line of the transmon. The duration of the Gaussian π-pulse is set to 26.7 ns. The readout probing pulse is produced by a Zürich Instruments SHFQA Quantum Analyzer and either applied to the common resonator feedline or via the charge line of the qubit [50]. Both ways result in the same experimental outcome in terms of cavity reset and assignment fidelity, but the latter removes most of a_{in} from the output for visualization purposes. The resulting output

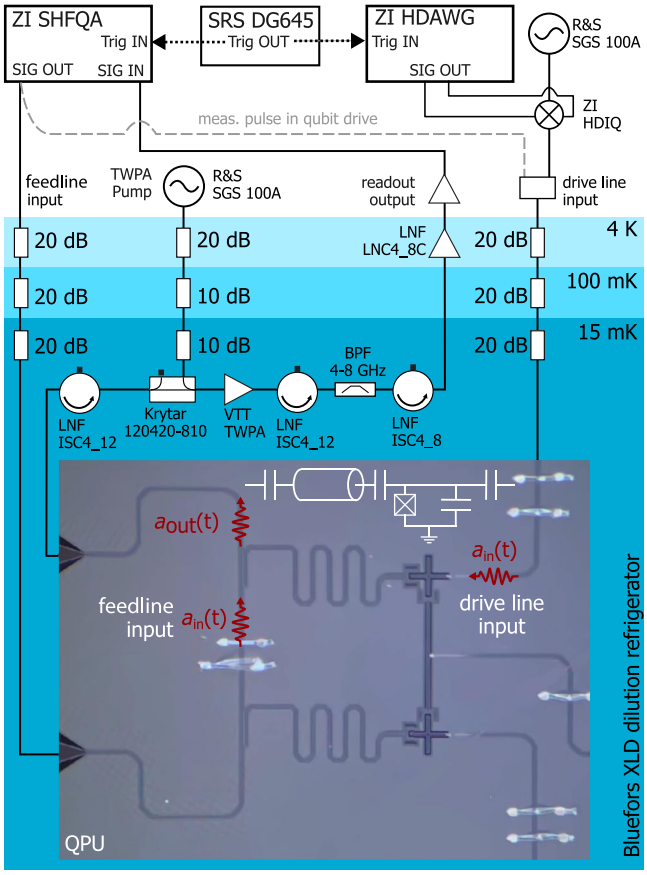

FIG. 7. Wiring diagram of the smooth readout experiment specifying the electronics and components. The readout input pulse $a_{in}(t)$ is synthesized with the quantum state analyzer (SHFQA) and is applied in two different possible configurations: through the feedline input or via the qubit drive. The readout signal $a_{out}(t)$ is amplified and then processed by the SHFQA. The baseband qubit control pulses are generated by HDAWG and upconverted to a carrier frequency. Microscope image of a quantum processing unit (QPU) with two transmon qubits. Only the top qubit is used for the experiment. Simplified circuit diagram of the transmon qubit coupled to the resonator (white).

signal $a_{out}(t)$ from the common feedline is initially amplified by a traveling wave parametric amplifier (TWPA) with a gain of around 10 dB. The TWPA is pumped by a continuous tone at 5.34 GHz with a power of about −110 dBm. After additional amplification at 4 K by a HEMT (Low Noise Factory LNF-LNC4-8C) and at room temperature the signal is detected by the SHFQA. The cold amplification stages are separated by two cryogenic isolators. The final detection steps include averaging and digital band-pass filtering when time traces are recorded, and weighted integration in case of single-shot measurements, see Appendix C. The detection efficiency of the setup is calibrated by using conventional power-spectral density measurements, see Refs. [5,51], and attains $\eta = 17\%$.

APPENDIX B: CALIBRATION OF NUMBER OF PHOTONS

The calibration of the photon number in the cavity requires a two-step procedure. During the first step, we calibrate the total gain of the system, which relates the magnitudes and phases of output and input signals at the SHFQA: $a_{out}(t) = s_{in}e^{-i\phi_{in}}a_{in}(t) + s_{cav}e^{-i\phi_{cav}}a(t)$, where s_{in} and ϕ_{in} are the amplitude and phase of transmission from the input port to the output port, and s_{cav} and ϕ_{cav} are the amplitude and phase of transmission from the cavity port to the output port. To find s_{cav} and ϕ_{cav} we apply rectangular pulses of variable amplitude and fit the decaying intra-cavity fields after the excitation. The s_{in} and ϕ_{in} coefficients are found by detecting the output signal for a very short 50 ns pulse, much shorter than κ^{-1}. In the single-ended driving configuration, i.e. excitation of the cavity through the readout line, $s_{cav} \approx s_{in}/2$ since the driving signal can travel directly to the output and half the signal leaving the cavity travels back to the input, with small corrections due to crosstalk and other loss channels. In the case of driving through the charge line of the qubit $s_{in} \ll s_{cav}$.

During the second step, we calibrate the dependence of the received signal power at the SHFQA input on the number of photons in the cavity. For that, at $t = -4$ μs the cavity is excited with a 4 μs long rectangular pulse. This pulse builds up the steady-state population of the intra-cavity field in about 1 μs. Right before the pulse is finished we deploy the standard Ramsey sequence to determine the ac-Stark shift of the qubit $\Delta_{AC} = 2\chi\langle n\rangle$ [52]. Two $\pi/2$ pulses with separation $T_R = 50$–500 ns are applied with

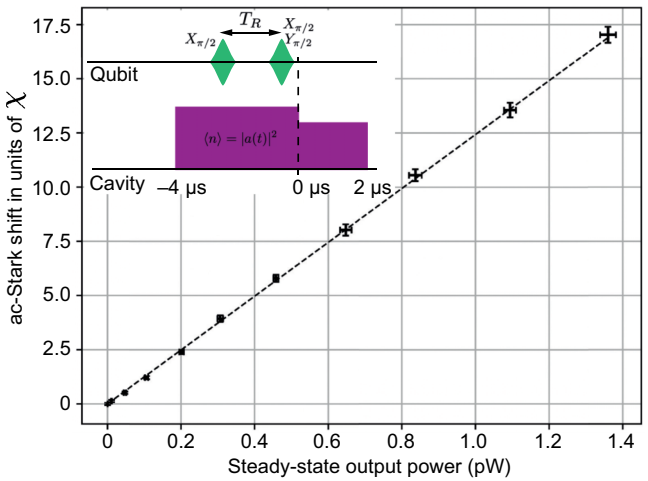

FIG. 8. Calibration of the intra-cavity photon number $\langle n(t)\rangle = |a(t)|^2$ by measuring the ac-Stark shift in a Ramsey experiment versus steady-state output power. Inset: the experimental pulse sequence. A long 4 μs cavity pulse builds up the steady-state population with variable magnitude, which overlaps with a Ramsey sequence at the end of the pulse. The qubit state is measured with a rectangular pulse of 2 μs duration.

10 MHz detuning from the 01 transition, followed by a 2 μs rectangular measurement pulse for the qubit state measurement. Figure 8 shows the linear dependence of the ac-Stark shift on the steady-state output power, which yields 12.4(1) photons per pW of detected power at the SHFQA.

APPENDIX C: SIGNAL ACQUISITION AND PROCESSING

The SHFQA converts the analog output signal of the cryostat in the band of (6.3 ± 1) GHz into a 2 GSa/s digital baseband I/Q signal. This signal comprises a_{out} at -260 MHz, the TWPA pump at -960 MHz and added wideband noise. We first remove the TWPA pump by applying a low-pass finite impulse response (FIR) filter designed to roll off beyond ± 860 MHz. We then shift the carrier frequency to zero by multiplication with $e^{-i\omega_{\mathrm{carrier}}t}$. We find the electrical delay of the setup and filtering using cross-correlation between $|a_T(t)|$ and $|a_{\mathrm{out},1}(t) - a_{\mathrm{out},0}(t)|$ in a qubit measurement. We also use this delay value to adjust the time axis of other measurements taken in the same hardware configuration. We find the amplitude s_{in} and phase ϕ_{in} of transmission from the input port to the output port and the amplitude s_{cav} and phase ϕ_{cav} of transmission from the cavity port to the output port by fitting $a_{\mathrm{out}}(t) = s_{\mathrm{in}}e^{-i\phi_{\mathrm{in}}}a_{\mathrm{in}}(t) + s_{\mathrm{cav}}e^{-i\phi_{\mathrm{cav}}}a_{\mathrm{thy}}(t)$, where a_{thy} is the output of the cavity predicted by the theoretical model. We solve this expression for a_{thy} to calculate $a(t)$. Finally, we apply a 20 to 50 MHz low-pass FIR filter to $a(t)$ and compensate for its delay.

APPENDIX D: THEORETICAL MODEL OF THE CAVITY RESPONSE

The model curves $a_{\mathrm{thy}}(t)$ in Figs. 1–4 are the result of a Lindblad master equation simulation of $\hat{H}_{\mathrm{tot}}$ for each qubit state with an additional driving term in the rotating frame at the carrier frequency:

$$\hat{H}_j(t) = \hbar\chi_j\hat{a}^+\hat{a} + \hbar\zeta_j(\hat{a}^+)^2\hat{a}^2 + \hbar a_{\mathrm{in}}(t)\hat{a} + \hbar\bar{a}_{\mathrm{in}}(t)\hat{a}^+.$$

Since this simulation is computationally expensive at the photon numbers involved, we approximate the problem by scaling the Kerr term by a factor of 10, the driving term by a factor of $1/\sqrt{10}$ and the size of the Hilbert space by a factor of 1/10, which gives reasonably accurate results.

APPENDIX E: QND-NESS OF THE MEASUREMENT

We have already shown that the measurement protocol is quantum non-demolition (QND) with respect to the cavity, bringing the final population back to the initial vacuum state. This ensures that the cavity does not interfere with future coherent operations by introducing qubit phase errors and detunings, and in future measurements by changing the signal to noise ratio. For example, a driven two-qubit transition with a Rabi frequency of 5 MHz will become off-resonant by $n\chi$, where n is the leftover population. For typical values in experiments around $n = 1$, this means that, even for very small values of $\chi \approx 0.3$ MHz as we have here, we expect about $(0.3/5)^2 \approx 0.4\%$ error in the gate, which is a major bottleneck for most systems. On the other hand, DRACHMA brings the photon population to below 0.01, which makes these effects negligible even for very large χ.

Another important consideration is the detrimental effect the readout can have on the state of the qubit. Note that unlike leakage and cavity errors, errors on readout qubits are generally included in error correcting codes. Nevertheless, for best performance, the qubit state should change neither by the end nor during the measurement. In both cases, this can result in qubit errors, while in the latter it can further result in cavity errors and also in readout errors.

Because of hybridization between the qubit (or qudit) and readout cavity states, DRACHMA can actually act via the very high sensitivity of the cavity to being in the wrong qubit state, covering a range of over 3 dB, as a sensor (or syndrome measurement) for qubit errors.

We first discuss the principal qubit error sources. (1) *Qubit driving* (X) *errors*: Since the resonator and qubit are typically detuned strongly (i.e. in GHz) and in the strongly dispersive regime, driven transitions are a (highly) off-resonant effect. It is well known that the qubit population error due to cavity driving roughly amounts to the Rabi probability $(\frac{ga_T}{(\omega_c-\omega_{01})^2})^2$. In our system, we expect that this error will be several orders of magnitude smaller than other error rates. In contrast, for much larger values of χ in the quasi-dispersive regime, such as those reported for fast readouts [5], the formula above gives an error estimate on the order of 1%. Another important consideration is that cavity reset protocols with sharp edges (such as Ref. [14]) will be more prone to excitation, while smooth pulses such as DRACHMA will behave more adiabatically and with narrower bandwidth. Reducing the bandwidth can also dramatically improve the predicatability of the input pulse [53]. (2) *Spurious transitions*: A similar but more poorly understood error comes from unexpected transitions between higher levels of the transmon and/or resonator, often outside of the rotating wave approximation. This is once again known to be a problem when leaving the (strongly) dispersive regime and/or when the measurement field is very significantly above the critical photon number [43,54]. As with off-resonant qubit driving, strong driving leads to diabatically populating avoided crossings without being able to return to the original state. For adiabatic (i.e. slow) or counter-diabatic (DRAG-like [55]) driving, this effect can be significantly suppressed, as we expect with our

smooth pulses. (3) *Qubit relaxation*: The error coming from relaxation is expected to be on the order of roughly $\Gamma_1 T$ for the $|1\rangle$ state. Hence this contributes about half of the assignment error, as can be seen in Fig. 5(c). For much faster measurement, this effect is expected to be considerably weaker, e.g. by using Purcell filters, increasing amplifier efficiency, or simultaneously increasing χ and κ. One should also note that little effect is expected from increasing the cavity population, as the Purcell effect is actually counter-intuitively reduced under strong driving [56]. Meanwhile, transmon-level dressing of the cavity will renormalize the bare decay rate as $\tilde{\kappa}$, which can be substituted easily into the effective transfer functions without reduction in coherence. (4) *Driven population mixing*: Spurious coherent population driving can be further exacerbated by decoherence of the adiabatic or diabatic field-dressed states. This is especially problematic with dephasing processes, first because higher level states will have dramatically increased energy level dispersion [57]. Such mixing events take one out of the dressed eigenstates of the measurement and therefore prevent the population from returning to the fiducial state. The mixing transfers the potentially pure state into an "entangled" state between cavity and transmon, where at least one of the two orthogonal transmon states is wrong. Meanwhile, no longer being in an adiabatic eigenstate of a_T, the cavity also fails to return to the vacuum. Because large photon population during the measurement results in significant hybridization with the qubit [58], the cavity is therefore extremely susceptible to dephasing (known or spurious) on the qubit. We plot via simulation the effect of qubit mixing on the leftover population in Fig. 9 for different rates of bare qubit decoherence. We see that loss of coherence has a dramatic effect on the ability to return to the cavity vacuum (y axis), while a similar, but less pronounced by about an order of magnitude, effect can prevent the transmon from returning to the fiducial state (x axis). For stronger driving, weaker dispersion, and shorter times, this effect can once again be expected to worsen since more population is driven to higher levels.

Interestingly, Fig. 9 allows us to bound the effect of decoherence on the QND-ness of the measurement. We can see that on the right side of the plot, where DRACHMA reduces the population to below 0.01 photons, there is approximately a quadratic relationship between photon and qubit error, with a tenfold decrease in photon population corresponding to a 100-fold decrease in the bound on qubit mixing. Given the experimentally observed depletion of the photon population in the cavity at below 0.01 photons, we can bound the effect of decoherence on the preservation of the qubit state, in this case at about 10^{-3}. In contrast, with standard readout protocols that stay closer to 1 photon at the end of the readout pulse, no meaningful bound can be placed on eigenstate mixing.

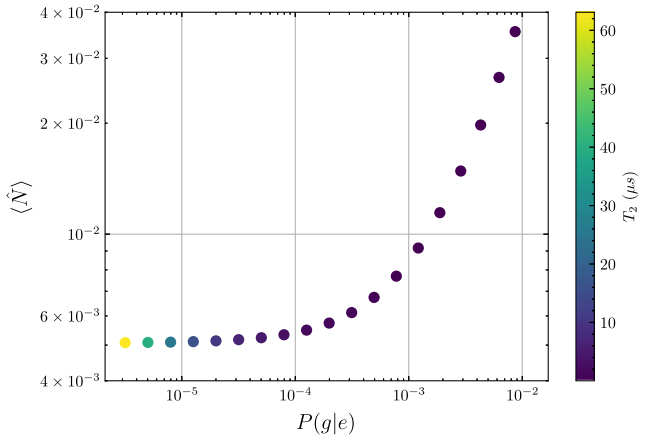

FIG. 9. Relationship between the leftover cavity population and the mixing error in the qubit. For each value of qubit decoherence, the measurement is simulated numerically, reaching a maximum near 100 photons, before being brought down by DRACHMA to around 0.01 photons. The x axis represents the probability of being in the excited qubit state when the system was initially in the ground. A very similar plot occurs with the states reversed. The y axis shows the cavity population immediately after the pulse finishes. The plots are calculated for 1000 ns with the same system parameters given in the main text.

APPENDIX F: DRACHMA FOR LONG READOUTS

Existing devices are commonly designed for cavity reset by natural decay rather than by optimal control. Since an additional delay of $T_{\text{hold}} > 9/\kappa$ is needed for the cavity population to decay 10^4-fold, this mandates fast cavities and readout pulse durations of many cavity lifetimes. Typical parameters are $\kappa^{-1} = 15$ ns, $T_p = 300$ ns, cf. Table I, and $2\chi = \kappa$. DRACHMA, with $a_T(t) = \sin^m(\pi t/T_p)$ used in the main text, is best for short readouts up to a few κ^{-1}. For longer readouts, a function with a larger mean value is a better choice, for example $a_T(t) = \text{erf}^m(t/t_r)\text{erf}^m((T_p - t)/t_d), t \in [0, T_p]$, which becomes a Gaussian-filtered rectangular pulse for $m = 1$.

In Fig. 10 we numerically compare the performance of a conventional Gaussian filtered pulse a_T and its DRACHMA version a_{in}. For the conventional pulse, we use $T_p = 300$ ns, $t_r = t_d = 10$ ns, $m = 1$. For its DRACHMA version, we use $T_p = 325$ ns, $t_r = 45$ ns, $t_d = 22.5$ ns and $n = 3$ to fulfill the smoothness conditions and keep the derivative terms small. The respective amplitudes are adjusted such that the maximum number of photons in the cavity is the same for both readouts. Both pulses achieve the same SNR, but while DRACHMA has reduced the number of photons in the cavity 10^4-fold at 320 ns, an additional hold time of 115 ns is required to reach that number by natural decay. While the advantage of DRACHMA is not as pronounced for these parameters, there is still a roughly 25% decrease in the aggregated measurement and cavity depletion times.

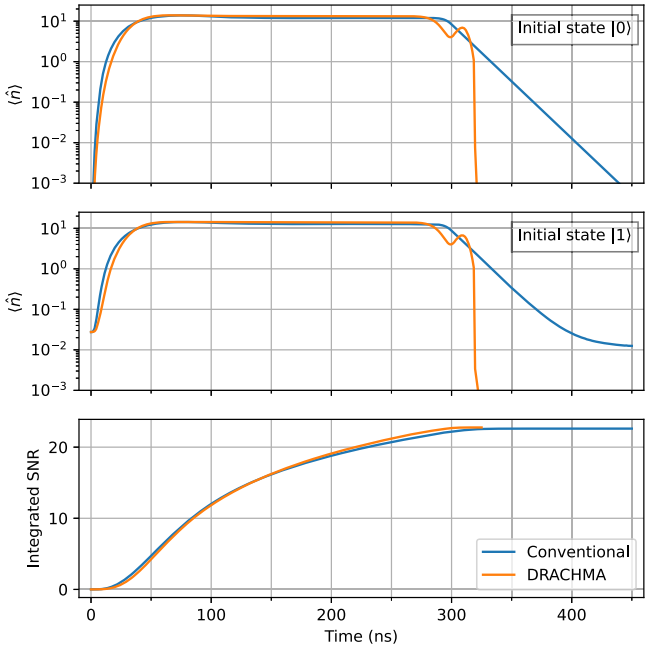

FIG. 10. Comparison of a conventional Gaussian-filtered rectangular measurement pulse and its DRACHMA version in case of a long $(20/\kappa)$ readout of a fast cavity. Both pulses achieve the same SNR in the same time and with the same maximum cavity occupation, but DRACHMA also depletes the cavity at the end of the pulse.

[1] A. Yu Kitaev, *Quantum Error Correction with Imperfect Gates* (Springer US, Boston, MA, 1997), pp. 181–188.

[2] A. G. Fowler, M. Mariantoni, J. M. Martinis, and A. N. Cleland, *Surface codes: Towards practical large-scale quantum computation*, Phys. Rev. A **86**, 032324 (2012).

[3] Steven M. Girvin, *Introduction to quantum error correction and fault tolerance*, SciPost Phys. Lect. Notes 70 (2023).

[4] M. Takita, A. D. Córcoles, E. Magesan, B. Abdo, M. Brink, A. Cross, J. M. Chow, and J. M. Gambetta, *Demonstration of weight-four parity measurements in the surface code architecture*, Phys. Rev. Lett. **117**, 210505 (2016).

[5] T. Walter, P. Kurpiers, S. Gasparinetti, P. Magnard, A. Potočnik, Y. Salathé, M. Pechal, M. Mondal, M. Oppliger, C. Eichler, and A. Wallraff, *Rapid high-fidelity single-shot dispersive readout of superconducting qubits*, Phys. Rev. Appl. **7**, 054020 (2017).

[6] B. Foxen *et al.*, *Demonstrating a continuous set of two-qubit gates for near-term quantum algorithms*, Phys. Rev. Lett. **125**, 120504 (2020).

[7] Q. Ficheux, L. B. Nguyen, A. Somoroff, H. Xiong, K. N. Nesterov, M. G. Vavilov, and V. E. Manucharyan, *Fast logic with slow qubits: Microwave-activated controlled-z gate on low-frequency fluxoniums*, Phys. Rev. X **11**, 021026 (2021).

[8] Youwei Zhao *et al.*, *Realization of an error-correcting surface code with superconducting qubits*, Phys. Rev. Lett. **129**, 030501 (2022).

[9] J. Gambetta, A. Blais, D. I. Schuster, A. Wallraff, L. Frunzio, J. Majer, M. H. Devoret, S. M. Girvin, and R. J. Schoelkopf, *Qubit-photon interactions in a cavity: Measurement-induced dephasing and number splitting*, Phys. Rev. A **74**, 042318 (2006).

[10] Zijun Chen *et al.*, *Exponential suppression of bit or phase errors with cyclic error correction*, Nature (London) **595**, 383 (2021).

[11] A D. Córcoles, M. Takita, K. Inoue, S. Lekuch, Z. K. Minev, J. M. Chow, and J. M. Gambetta, *Exploiting dynamic quantum circuits in a quantum algorithm with superconducting qubits*, Phys. Rev. Lett. **127**, 100501 (2021).

[12] S. Krinner, N. Lacroix, A. Remm, A. Di Paolo, E. Genois, C. Leroux, C. Hellings, S. Lazar, F. Swiadek, J. Herrmann, G. J. Norris, C. K. Andersen, M. Müller, A. Blais, C. Eichler, and A. Wallraff, *Realizing repeated quantum error correction in a distance-three surface code*, Nature (London) **605**, 669 (2022).

[13] Y. Sunada, K. Yuki, Z. Wang, T. Miyamura, J. Ilves, K. Matsuura, P. A. Spring, S. Tamate, S. Kono, and Y. Nakamura, *Photon-noise-tolerant dispersive readout of a superconducting qubit using a nonlinear purcell filter*, PRX Quantum **5**, 010307 (2024).

[14] D T. McClure, H. Paik, L S. Bishop, M. Steffen, J. M. Chow, and J. M. Gambetta, *Rapid driven reset of a qubit readout resonator*, Phys. Rev. Appl. **5**, 011001 (2016).

[15] C. C. Bultink, M. A. Rol, T. E. O'Brien, X. Fu, B. C. S. Dikken, C. Dickel, R. F. L. Vermeulen, J. C. de Sterke, A. Bruno, R. N. Schouten, and L. DiCarlo, *Active resonator reset in the nonlinear dispersive regime of circuit qed*, Phys. Rev. Appl. **6**, 034008 (2016).

[16] A. Bengtsson, P. Vikstål, C. Warren, M. Svensson, X. Gu, A. F. Kockum, P. Krantz, C. Križan, D. Shiri, I.-M. Svensson, G. Tancredi, G. Johansson, P. Delsing, G. Ferrini, and J. Bylander, *Improved success probability with greater circuit depth for the quantum approximate optimization algorithm*, Phys. Rev. Appl. **14**, 034010 (2020).

[17] A. Blais, A. L. Grimsmo, S. M. Girvin, and A. Wallraff, *Circuit quantum electrodynamics*, Rev. Mod. Phys. **93**, 025005 (2021).

[18] S. M. Rytov, Y. A. Kravtsov, and V. I. Tatarskii, *Principles of Statistical Radiophysics 2: Correlation Theory of Random Processes* (Springer-Verlag, Berlin Heidelberg, 1988).

[19] J. M. C. Duhamel, *Mémoir sur les vibrations d'un système quelconque de points materiels*, J. L'Ecole Polytech. **23**, 1 (1834), https://gallica.bnf.fr/ark:/12148/bpt6k4336791

[20] M. J. Collett and C. W. Gardiner, *Squeezing of intracavity and traveling-wave light fields produced in parametric amplification*, Phys. Rev. A **30**, 1386 (1984).

[21] B. Yurke, *Input-Output Theory* (Springer-Verlag, Berlin Heidelberg, 2004).

[22] F. Motzoi, L. Buchmann, and C. Dickel, *Simple, smooth and fast pulses for dispersive measurements in cavities and quantum networks*, arXiv:1809.04116.

[23] J. Heinsoo, C. K. Andersen, A. Remm, S. Krinner, T. Walter, Y. Salathé, S. Gasparinetti, J.-C. Besse, A. Potočnik, A. Wallraff, and C. Eichler, *Rapid high-fidelity multiplexed readout of superconducting qubits*, Phys. Rev. Appl. **10**, 034040 (2018).

[24] M. Boissonneault, J. M. Gambetta, and A. Blais, *Improved superconducting qubit readout by qubit-induced nonlinearities*, Phys. Rev. Lett. **105**, 100504 (2010).
[25] J. Gambetta, W. A. Braff, A. Wallraff, S. M. Girvin, and R. J. Schoelkopf, *Protocols for optimal readout of qubits using a continuous quantum nondemolition measurement*, Phys. Rev. A **76**, 012325 (2007).
[26] E. A. Sete, J. M. Martinis, and A. N. Korotkov, *Quantum theory of a bandpass purcell filter for qubit readout*, Phys. Rev. A **92**, 012325 (2015).
[27] E. Jeffrey, D. Sank, J Y. Mutus, T C. White, J. Kelly, R. Barends, Y. Chen, Z. Chen, B. Chiaro, A. Dunsworth, A. Megrant, P J J. O'Malley, C. Neill, P. Roushan, A. Vainsencher, J. Wenner, A N. Cleland, and J. M. Martinis, *Fast accurate state measurement with superconducting qubits*, Phys. Rev. Lett. **112**, 190504 (2014).
[28] J. Gough and M. R. James, *The series product and its application to quantum feedforward and feedback networks*, IEEE Trans. Autom. Control **54**, 2530 (2009).
[29] N. T. Bronn, Y. Liu, J. B. Hertzberg, A. D. Córcoles, A. A. Houck, J. M. Gambetta, and J. M. Chow, *Broadband filters for abatement of spontaneous emission in circuit quantum electrodynamics*, Appl. Phys. Lett. **107**, 172601 (2015).
[30] J. Kerckhoff, L. Bouten, A. Silberfarb, and H. Mabuchi, *Physical model of continuous two-qubit parity measurement in a cavity-QED network*, Phys. Rev. A **79**, 024305 (2009).
[31] N. Roch, M E. Schwartz, F. Motzoi, C. Macklin, R. Vijay, A W. Eddins, A N. Korotkov, K B. Whaley, M. Sarovar, and I. Siddiqi, *Observation of measurement-induced entanglement and quantum trajectories of remote superconducting qubits*, Phys. Rev. Lett. **112**, 170501 (2014).
[32] C. Dickel, J. J. Wesdorp, N. K. Langford, S. Peiter, R. Sagastizabal, A. Bruno, B. Criger, F. Motzoi, and L. DiCarlo, *Chip-to-chip entanglement of transmon qubits using engineered measurement fields*, Phys. Rev. B **97**, 064508 (2018).
[33] L. Martin, F. Motzoi, H. Li, M. Sarovar, and K. B. Whaley, *Deterministic generation of remote entanglement with active quantum feedback*, Phys. Rev. A **92**, 062321 (2015).
[34] F. Motzoi, K. B. Whaley, and M. Sarovar, *Continuous joint measurement and entanglement of qubits in remote cavities*, Phys. Rev. A **92**, 032308 (2015).
[35] R. Dassonneville, T. Ramos, V. Milchakov, L. Planat, É Dumur, F. Foroughi, J. Puertas, S. Leger, K. Bharadwaj, J. Delaforce, C. Naud, W. Hasch-Guichard, J J. García-Ripoll, N. Roch, and O. Buisson, *Fast high-fidelity quantum nondemolition qubit readout via a nonperturbative cross-Kerr coupling*, Phys. Rev. **10**, 011045 (2020).
[36] S. Touzard, A. Kou, N. E. Frattini, V. V. Sivak, S. Puri, A. Grimm, L. Frunzio, S. Shankar, and M. H. Devoret, *Gated conditional displacement readout of superconducting qubits*, Phys. Rev. Lett. **122**, 080502 (2019).
[37] *Google Quantum AI, Exponential suppression of bit or phase errors with cyclic error correction*, Nature (London) **595**, 383 (2021).
[38] C. K. Andersen, A. Remm, S. Lazar, S. Krinner, N. Lacroix, G. J. Norris, M. Gabureac, C. Eichler, and A. Wallraff, *Repeated quantum error detection in a surface code*, Nat. Phys. **16**, 875 (2020).
[39] F. Swiadek, R. Shillito, P. Magnard, A. Remm, C. Hellings, N. Lacroix, Q. Ficheux, D. C. Zanuz, G. J. Norris, A. Blais, S. Krinner, and A. Wallraff, *Enhancing dispersive readout of superconducting qubits through dynamic control of the dispersive shift: Experiment and theory*, PRX Quantum **5**, 040326 (2024).
[40] P. A. Spring, L. Milanovic, Y. Sunada, S. Wang, A. F. van Loo, S. Tamate, and Y. Nakamura, *Fast multiplexed superconducting-qubit readout with intrinsic purcell filtering using a multiconductor transmission line*, PRX Quantum **6**, 020345 (2025).
[41] Pavel D. Kurilovich, Thomas Connolly, Charlotte G. L. Bøttcher, Daniel K. Weiss, Sumeru Hazra, Vidul R. Joshi, Andy Z. Ding, Heekun Nho, Spencer Diamond, Vladislav D. Kurilovich, Wei Dai, Valla Fatemi, Luigi Frunzio, Leonid I. Glazman, and Michel H. Devoret, *High-frequency readout free from Transmon multi-excitation resonances*, arXiv:2501.09161.
[42] J. Gambetta, A. Blais, M. Boissonneault, A. A. Houck, D. I. Schuster, and S. M. Girvin, *Quantum trajectory approach to circuit QED: Quantum jumps and the zeno effect*, Phys. Rev. A **77**, 012112 (2008).
[43] M. F. Dumas, B. Groleau-Paré, A. McDonald, M. H. Muñoz-Arias, C. Lledó, B. D'Anjou, and A. Blais, *Measurement-induced transmon ionization*, Phys. Rev. **14**, 041023 (2024).
[44] M. Keller, *Cavity-qed with single trapped ions*, Contemp. Phys. **63**, 1 (2022).
[45] S. Garcia, M. Stammeier, J. Deiglmayr, F. Merkt, and A. Wallraff, *Single-shot nondestructive detection of Rydberg-atom ensembles by transmission measurement of a microwave cavity*, Phys. Rev. Lett. **123**, 193201 (2019).
[46] H. Keßler, P. Kongkhambut, C. Georges, L. Mathey, J. G. Cosme, and A. Hemmerich, *Observation of a dissipative time crystal*, Phys. Rev. Lett. **127**, 043602 (2021).
[47] M. Aspelmeyer, T. J. Kippenberg, and F. Marquardt, *Cavity optomechanics*, Rev. Mod. Phys. **86**, 1391 (2014).
[48] V. Ranjan, J. O'Sullivan, E. Albertinale, B. Albanese, T. Chanelière, T. Schenkel, D. Vion, D. Esteve, E. Flurin, J. J. L. Morton, and P. Bertet, *Multimode storage of quantum microwave fields in electron spins over 100 ms*, Phys. Rev. Lett. **125**, 210505 (2020).
[49] L. M. K. Vandersypen and M. A. Eriksson, *Quantum computing with semiconductor spins*, Phys. Today **72**, 38 (2019).
[50] J. Ikonen, J. Goetz, J. Ilves, A. Keränen, A. M. Gunyho, M. Partanen, K. Y. Tan, D. Hazra, L. Grönberg, V. Vesterinen, S. Simbierowicz, J. Hassel, and M. Möttönen, *Qubit measurement by multichannel driving*, Phys. Rev. Lett. **122**, 080503 (2019).
[51] C. C. Bultink, B. Tarasinski, N. Haandbæk, S. Poletto, N. Haider, D. J. Michalak, A. Bruno, and L. DiCarlo, *General method for extracting the quantum efficiency of dispersive qubit readout in circuit qed*, Appl. Phys. Lett. **112**, 092601 (2018).
[52] F. R. Ong, M. Boissonneault, F. Mallet, A. Palacios-Laloy, A. Dewes, A. C. Doherty, A. Blais, P. Bertet, D. Vion, and D. Esteve, *Circuit QED with a nonlinear resonator: ac-stark shift and dephasing*, Phys. Rev. Lett. **106**, 167002 (2011).

[53] J. J. Sørensen, J. S. øNyemann, F. Motzoi, J. Sherson, and T. Vosegaard, *Optimization of pulses with low bandwidth for improved excitation of multiple-quantum coherences in nmr of quadrupolar nuclei*, J. Chem. Phys. **152**, 054104 (2020).

[54] M. Malekakhlagh, W. Shanks, and H. Paik, *Optimization of the resonator-induced phase gate for superconducting qubits*, Phys. Rev. A **105**, 022607 (2022).

[55] L. S. Theis, F. Motzoi, S. Machnes, and F. K. Wilhelm, *Counteracting systems of diabaticities using drag controls: The status after 10 years*, Europhys. Lett. **123**, 60001 (2018).

[56] E. A. Sete, J. M. Gambetta, and A. N. Korotkov, *Purcell effect with microwave drive: Suppression of qubit relaxation rate*, Phys. Rev. B **89**, 104516 (2014).

[57] F. A. Cárdenas-López, B. Li, A. Lupascu, and F. Motzoi, *Universal pulses for superconducting qudit ladder gates*, PRX Quantum **6**, 030357 (2025).

[58] A. Blais, R.-S. Huang, A. Wallraff, S. M. Girvin, and R. J. Schoelkopf, *Cavity quantum electrodynamics for superconducting electrical circuits: An architecture for quantum computation*, Phys. Rev. A **69**, 062320 (2004).